

Percolation phenomena in polymer nanocomposites

Moises Oviedo Mendoza, Edna M. Valenzuela-Acosta, Evgen Prokhorov*, Gabriel Luna-Barcenas, Siva Kumar-Krishnan

Cinvestav del IPN, Unidad Querétaro; Libramiento norponiente 2000, Fracc. Real de Juriquilla, Querétaro, Qro.76230, México

*Corresponding author. Tel: (+52) 442-2119921; E-mail: prokhorov@cinvestav.mx

Received: 10 August 2015, Revised: 15 December 2015 and Accepted: 18 March 2016

ABSTRACT

In this work, we report the relationship between the electrical conductivity and nanoparticle effective surface area with functional properties of polymer-metal and polymer-clay nanocomposites. Conductivity of the nanocomposite strongly depends upon metal/clay nanoparticle size and concentration that ultimately dictate where the system percolates. Knowledge of percolation properties allows the design of functional nanocomposites for biomedical and sensors applications. Herein we report the successful production of three functional chitosan-metal/clay nanocomposites: a) chitosan-Ag films with antibacterial properties, b) chitosan-Au potentiometric sensor for detection of Cu^{++} and c) chitosan-nanoclay potentiometric sensor for detection of NO_3^- . For all these applications the best functional performance of nanocomposites has been observed when NPs concentration increases and approaches the percolation threshold. The obtained relationship between electrical percolation threshold and functional properties of polymer nanocomposites is of primary importance in the design of high-performance applications. Copyright © 2016 VBRI Press.

Keywords: Chitosan; nanocomposites; percolation; antibacterial properties; potentiometric sensor.

Introduction

In recent decades natural polymers with inorganic nanoparticle composites have attracted increasing attention because of their unique properties emerging from the combination of organic and inorganic hybrid materials. Polymers are a suitable matrix material for stabilization and homogeneous nanoparticles (NPs) dispersion in the polymer environment. Properties of nanocomposites essentially depend upon the high surface area of the NPs, which in turn depend upon the size and concentration of NPs. Generally, the resultant nanocomposites display enhanced optical, mechanical, magnetic and electric properties. Due to such properties polymer-nanoparticles composites find applications in novel electrical, optical, magnetic, catalytic, biomedical and sensing technologies [1, 2].

Different routes of synthesis of polymer-NPs composites have been proposed; the most relevant are: intercalation of nanoparticles with the polymer from solution; *in situ* intercalative polymerization; melt intercalation; direct mixture of polymer and particles; *in situ* polymerization; sol-gel process; and chemical reduction of precursors by reducing agents in polymer solution, etc. [1, 2].

Synthesis method directly affects nanocomposite properties such as nanoparticle dimension, shape, size and concentration, interaction with polymer matrix, among others. Dimensional features of NPs can be obtained from TEM, SEM or AFM measurements but the fine-control of NPs concentration is still a challenge. Additionally, one of

the most important questions of nanotechnology is how to compare properties of nanocomposites (with the same polymer matrix and type of nanoparticles) obtained using different methods of preparation (precursors, reducing agents, temperature, etc.). Another problem arises on how to optimize NPs concentration with the highest surface area in the composites while avoiding agglomeration.

Polysaccharides, polyanilines, polystyrenes, and epoxies, among others are used as nanocomposite's matrix; they exhibit highly insulating dielectric behavior and a very high electrical resistivity. Conversely most nanoparticles such as metallic, carbon nanotubes, and clay exhibit low resistivity. Consequently a mixture of high and low resistivity materials (characterized by their electrical conductivity σ , and dielectric constant ϵ) will exhibit a percolation phenomenon: the conductivity of the nanocomposite will change from the one of the dielectric component to the one of the metallic component; the dielectric constant will diverge near the percolation threshold [3, 4].

According to percolation theory, the DC conductivity above the percolation threshold can be characterized by a simple power law [4, 5]:

$$\sigma \propto (p - p_c)^t, \quad (1)$$

where, p represents the volume fraction of conductivity phase, p_c is the critical fraction at the percolation threshold and t is a critical exponent which only depends on the dimensionality of the percolation system; values are

typically *ca.* 1.3 and 2.0 for two and three-dimensions, respectively [4]. For the nanocomposite system, the percolation phenomenon is observed when conducting particles of the disperse phase come into close contact with each other; a continuous path extends throughout the system as the volume fraction of the disperse phase approaches a critical value p_c [6, 7].

It is noteworthy that polymer nanocomposites are often characterized as a function of weight percent (wt. %) instead volume fraction (see, for example [8-11]) due to the following particle complexation: there exists an interfacial shell between metallic NPs that promote electric channeling before the metal particles have actual physical contact [12, 13]. These interfacial shells may depend upon the method of nanocomposite preparation. Therefore, polymer-NPs composite should be regarded as a material behaving as "complex particles" with a dimension higher than that of NPs; the volume fraction differs from the one of NPs embedded in the polymer matrix [12]. For this reason wt % of NPs better characterizes percolation properties of nanocomposites allowing comparing nanocomposites obtained by different preparation methods.

Application of many nanocomposites, as mention above, are based upon the high effective surface area of the NPs, which after percolation threshold can decrease due to agglomeration of NPs in clusters that decrease the effectiveness of nanocomposites. Therefore, optimum NPs concentration in polymer-metal/clay nanocomposites must be close to the percolation threshold concentration before agglomeration overwhelms the high surface area of the NPs.

The aim of this work is to confirm that the effective surface area of metal/clay NPs on chitosan-based nanocomposites is correlated with the percolation threshold. This correlation may be used for the smart design of: 1) antibacterial films for the biomedical field, and 2) potentiometric sensors for heavy metal and anion detection. It is known that these chitosan-based nanocomposites strongly depend upon effective surface area of NPs. Chitosan is a polysaccharide that has been successfully applied in a wide spectra of applications including medicine, food and chemical engineering, pharmaceutical, sensing and agriculture due to its biocompatibility and biodegradability, intrinsic antibacterial nature and ability to be prepared in various physical forms [14, 15].

In this work, properties of chitosan (CS)-based nanocomposites with metallic silver (AgNPs), gold (AuNPs) and clay nanoparticles have been investigated. The relationship between electrical properties and optimum concentration of NPs for application in biomedicine and sensors has been also assessed.

Experimental

Materials synthesis

Chitosan medium molecular weight ($M_w=300$ kDa and 82 % of degree of deacetylation) was purchased from Sigma-Aldrich. $AgNO_3$, $H AuCl_4$ and acetic acid were also purchased from Sigma Aldrich and were used as received. Sodium Bentonite extracted from Cuencamé Durango, México was purchased from FEMISA SA.

Chitosan solutions were obtained by dissolving 1 wt. % of CS powder in 1% aqueous acetic acid solution and was subsequently stirred to promote dissolution.

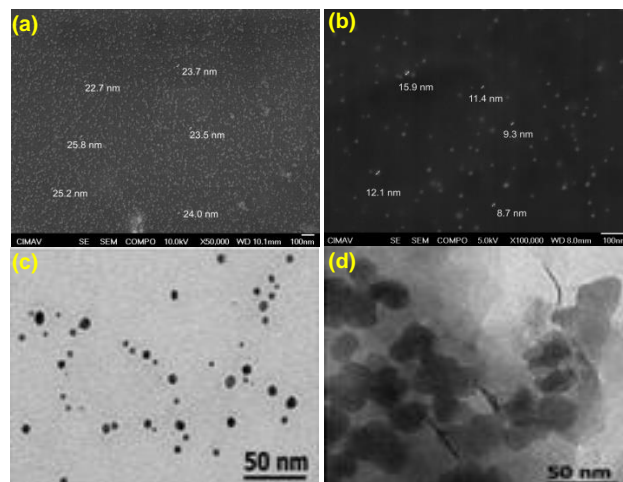


Fig. 1. SEM images of (a) CS-AgNPs (1 wt. %) obtained by dispersion NPs in CS solution and (b) CS-AuNPs (0.75 wt. %). TEM images of: (c) CS-AgNPs obtained by chemical reduction (0.5 wt. %) and CS-clay (8 wt. %) nanocomposites.

CS/AgNPs nanocomposites were prepared by two different methods: a) direct mixture of polymer and AgNP's powder (with different wt. % respect to CS dry-base) in a chitosan solution; b) chemical reduction of silver precursor $AgNO_3$ with different mM concentrations in a chitosan solution which was magnetically stirred at 95 °C, then allowed to react for an additional 8 hours. According to SEM and TEM measurements the dimensions of AgNPs in cases a) and b) were *ca.* 25 nm and 4-7 nm, respectively (**Fig. 1(a, c)**).

AuNPs were prepared by chemical reduction of $H AuCl_4$ at different concentrations by adding a sodium citrate solution to a solution that is kept at constant temperature (96 °C) and stirring. Finally, the CS/AuNPs nanocomposite was obtained by adding the gold nanoparticles to the chitosan aqueous acidic solution under vigorous stirring. According to SEM measurements dimension of AuNPs were in the range 8-14 nm (**Fig. 1b**).

Chitosan/bentonite nanocomposites (with layer dimension *ca.* 32 nm x 26 nm according TEM measurements, (**Fig. 1d**) with different wt. % were prepared by adding bentonite to the chitosan solution.

CS nanocomposites films (with thickness *ca.* 30 μ m) were obtained by the solvent casting method pouring the final solution into a plastic Petri dish and allowing the solvent to evaporate for 24 h at 60°C. Films were gold-sputtered on both sides to serve as contacts.

Characterizations

Film's morphology and NPs dimension were analyzed by JEOM JSM7401F field emission scanning electron microscope (SEM) and JEOL JEM-1010 transmission electron microscope (TEM). The weight percent of NPs in the chitosan film was obtained by energy dispersive analysis (EDS).

DC conductivity of nanocomposites as function of NPs concentration have been obtained by impedance

measurements using Agilent Precision Impedance Analyzer 4249A in the frequency range from 40 Hz to 110 MHz. The amplitude of the measuring signal was 100 mV. The DC resistance (R_{dc}) was obtained from the intersection of the semicircle and the real-part axis on the impedance plane (at $Z'' = 0$) as was described in [11, 16]. DC conductivity (σ_{dc}) can be calculated by the following relationship: $\sigma_{dc} = d / (R_{dc} \times A)$ where d is film thickness and A is the area of film, respectively (which have been measured for every sample using Mitutoyo Micrometers).

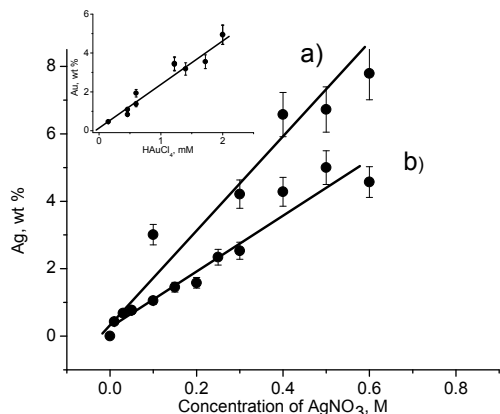


Fig. 2. Dependence of AgNPs wt. % in the films on the AgNO_3 concentration in the solution: (a) direct reduction of AgNO_3 precursor in chitosan solution and (b) using chemical reduction with ascorbic acid and sodium citrate as reducing and stabilizing agents respectively. Insert shows dependence of AuNPs wt % on in CS-AuNPs films on the HAuCl_4 concentration (EDS analysis).

Results and discussion

As previously mentioned, percolation phenomena is studied for our polymer nanocomposites as a function of wt % instead of volume fraction as shown in **Fig. 2**. Here we show the dependence of AgNPs wt % obtained in films by EDS analysis on molar concentration of AgNO_3 in solution from which films have been prepared. Films were prepared using two different reduction methods: a) reduction of silver precursor AgNO_3 at different mM concentration in chitosan solution and b) using the well-known method of chemical reduction with ascorbic acid and sodium citrate as reducing and stabilizing agents, respectively [16]. EDS analysis shows that the weight percent of metallic silver in the CS film linearly varies with molar concentration and it is strongly dependent on the method of preparation. Insert on **Fig. 2** shows dependence of AuNPs wt % on in chitosan-gold nanoparticles films. In this regard, we propose a method that allows comparison of nanocomposites properties obtained by different synthesis methods; this comparison is crucial for investigating percolation phenomena and further nanocomposite applications.

Fig. 3 shows the DC electrical conductivity of different CS-based nanocomposites obtained from impedance measurements as a function of the NPs/bentonite wt %. **Fig. 3a** corresponds to CS-AgNPs composites obtained by the two methods mentioned before. **Fig. 3b** shows DC conductivity obtained in CS-AuNPs and **Fig. 3c** shows CS/bentonite nanocomposites. Neat chitosan exhibits low ionic conductivity that can be related to the presence of

small concentration of conductive species (due to water absorption) in the form of OH^- and H^+ ions [17]. An abrupt increase in conductivity by increasing NPs wt % and a subsequent saturation is typically observed for percolation phenomena due to increasing of NPs concentration. It is noteworthy that CS-AgNPs and CS-AuNPs nanocomposites exhibits relatively low conductivity even in the saturation region. Such effect has been observed in polymer-AgNPs composites and it is traceable to the absorption polymer chains onto AgNPs surface that act as the dielectric barrier [18]. In other words, there is an interfacial shell between the nanoparticles, which depends upon the preparation method; this phenomenon makes complete direct contact between NPs highly unlikely. Methods based on the determination of wt % of NPs using EDS analysis help disregard these interfacial shells allowing comparison of nanocomposites obtained by different preparation methods.

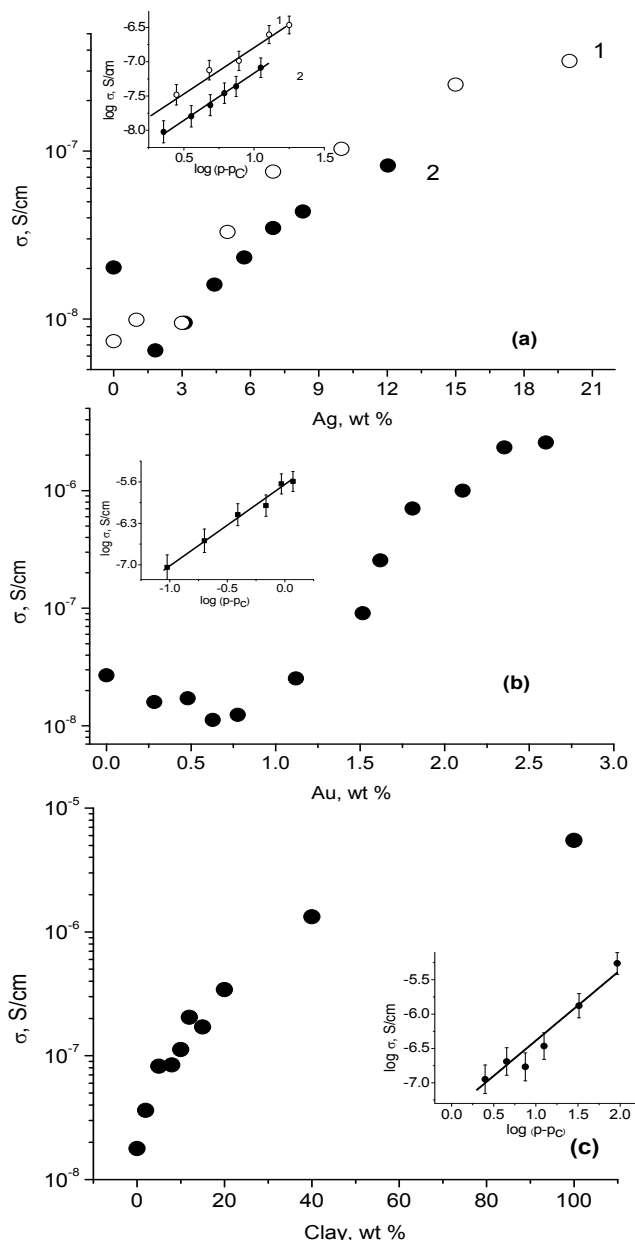


Fig. 3. DC electrical conductivity of a) CS-AgNPs films b) CS-AuNPs films and c) CS-bentonite films as a function of NPs wt. % (last data from ref. [32]). Inserts show a double log-log plot of the electrical conductivity versus $p-p_c$.

It is noteworthy that at low concentration of AgNP and AuNPs a decreasing in conductivity was observed. The decrease of conductivity at low concentration of nanoparticles has been explained by the strong interactions of AgNPs and AuNPs with OH and NH_3^+ groups of CS film, which in turns decrease the free H^+ and OH^- ; these species are responsible for the conduction in CS [19].

The insets in Fig. 3 show the log-log dependence of the conductivity of the CS composites on $p-p_c$, which according to equation (1) must exhibit linear dependence. The least-square fitting analysis according to equation (1) above percolation results in a percolation threshold of 2.66 ± 0.54 wt % for silver nanoparticles in films obtained by direct dispersion of AgNPs in chitosan solution; 0.85 ± 0.31 wt. % for nanocomposite obtained by chemical reduction of AgNO_3 precursor in chitosan solution; 1.43 ± 0.28 wt. % for CS-AuNPs nanocomposites and 8 ± 2.5 wt % of clay for CS- bentonite films.

The values of the percolation threshold concentration obtained on different CS-based nanocomposites correlate well with those of theoretical calculation and experiments on tin-polypropylene nanocomposites reported previously [12]. According to ref. [12], the percolation threshold of metal-polymer composites decreases rapidly with decreasing metal particle size. Similar results have been obtained in our work. CS-bentonite nanocomposite with dimensions of bentonite layer *ca.* $32 \text{ nm} \times 26 \text{ nm}$ exhibits a percolation threshold of 8 ± 2.5 wt %. AgNPs (AgNPs and AuNPs have sphere like shapes) in films obtained by direct dispersion of powder in chitosan solution are 25 nm with a percolation threshold of 2.66 ± 0.54 wt %. AuNPs in CS films are 9-14 nm in size and a percolation threshold of 1.43 ± 0.28 wt. %. AgNPs in films obtained by chemical reduction are 4-7 nm with a percolation threshold of 0.85 ± 0.31 wt. %. Dependence of percolation threshold on dimensions of NPs obtained in this work is shown on Fig. 4.

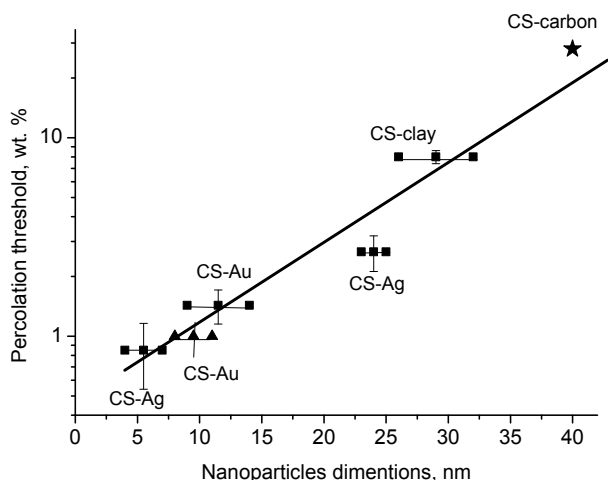


Fig. 4. Dependence of percolation threshold on dimensions of NPs. Squares represents data for CS-AgNPs, CS-AuNPs and CS-clay (this work); star corresponds to CS-carbon nanoparticles (ref. [20]); triangles correspond to CS-AuNPs obtained by chemical reduction of HAuCl_4 in chitosan solution (ref. [21]). The straight line is a guide to the eye.

Fig. 4 includes data for chitosan-carbon nanoparticles (star) reported in ref. [20] and CS-AuNPs (triangles)

obtained by chemical reduction of HAuCl_4 in chitosan solution [21]. This dependence shows a strong correlation between percolation threshold and NPs size.

The obtained relationship between impedance measurements and critical percolation concentration of NPs are of primary importance in the design and optimization of such nanocomposite for different applications.

Now let's examine three applications of CS-based nanocomposites, which were designed considering their percolation phenomena.

It has been previously reported that CS-AgNPs can be used as antibacterial biomaterial [22, 23]. In our work the antibacterial activity of both CS-AgNPs nanocomposites (obtained by directly dissolving of AgNPs powder and by chemical reduction) with different concentration of NPs were tested on Gram-positive and Gram-negative bacteria, namely *Staphylococcus aureus* and *Escherichia coli* respectively [23].

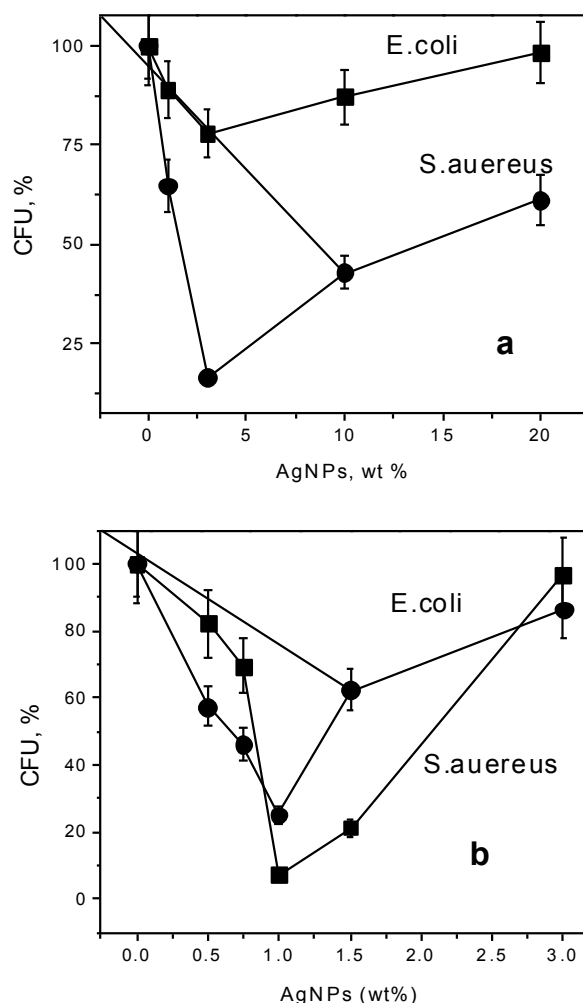


Fig. 5. Relative change of CFU (colony-forming-unit) versus AgNPs wt % for CS-AgNPs nanocomposites with a) Ag powder and b) AgNPs obtained by chemical reduction after 48 h of culture.

The antibacterial effect of both Ag nanocomposites films against *Staphylococcus aureus* and *Escherichia coli* incubated after 48 h is shown in Fig. 5. From this figure it can be observed that the best antibacterial effect for both nanocomposites occur at a critical concentration dictated by the percolation threshold concentration (Fig. 2a).

CS-AgNP films with *ca.* 2.5 wt. % of Ag powder (**Fig. 5a**) and composites obtained by chemical reduction (**Fig. 5b**) with *ca.* 1 wt % showed minimum Colony-Forming-Units (CFU), i.e. maximum bactericidal effect. These values correlate well with the percolation thresholds obtained from electrical measurements (2.66 ± 0.54 wt % and 0.85 ± 0.31 wt. %). Above this critical concentration the antibacterial activity decreases against both Gram-positive *Staphylococcus aureus* and Gram-negative *Escherichia coli*.

Exact mechanism of antibacterial properties of CS-AgNPs is still not known; however, ref. [24] proposes that the dominating factor is the direct contact of bacteria with nanoparticles. The percolation phenomena help explain the observed maximum bactericide activity of the CS/AgNP's composites, i.e. once the system percolates, a continuous physical path is formed in which the current can flow; thus decreasing the effective surface area of nanoparticles. Additionally, at higher silver concentrations clusters start to appear which further decrease the surface area of nanoparticles and effective contact AgNPs with bacteria [23].

Another example of chitosan-nanoparticles application that has been proposed in the literature is the use of CS-AuNPs for detection of heavy metals such as Cu^{+2} , Cd^{+2} and Pb^{+2} [25-27]. Refs. [25, 26] proposed that CS-AuNPs can be used as sensors for detection of heavy metals based upon the Surface Plasmon resonance (SPR); ref. [26] proposes a sensor based upon cyclic voltammetry by investigating the role of pH of the chitosan solution precursor and its sensitivity. Ref. [26] assesses the effect of molar relation between CS and AuNPs on the sensitivity of a SPR sensor. In our work, potentiometric measurements are carried out using a graphite-epoxy electrode covered by CS-AuNPs films with different wt. % of nanoparticles for detection of Cu^{2+} ions.

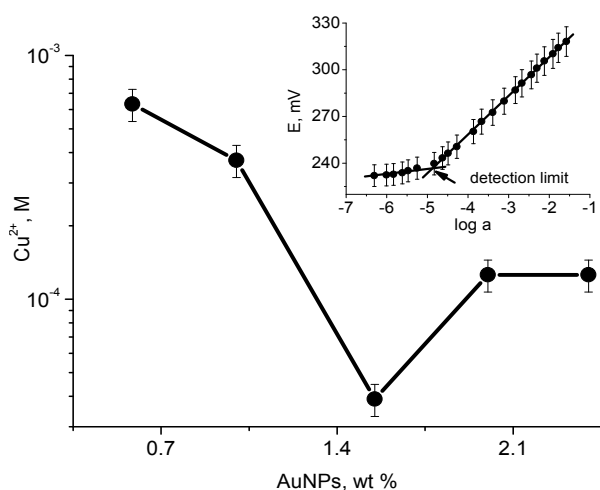


Fig. 6. Detection limit dependence of CS-AuNPs film electrode toward Cu^{2+} as a function of AuNPs concentration. Insert shows electrode potentiometric response to Cu^{2+} with 1.55 wt % AuNPs film. a is ion activity calculated according to ref. [29].

Fig. 6 shows dependence of detection limit of electrode for Cu^{2+} ions on the wt. % of AuNPs films. The detection limit of electrodes was taken at the point of intersection of the two asymptotic behaviors of the calibration curve, as

recommended by IUPAC (see insert on **Fig. 4**) [28]. As one can see the best detection limit can be obtained at 1.55 wt % of AuNPs films, which is close to the percolation threshold (1.43 ± 0.28 wt. %).

The polycationic nature of chitosan enables attachment of the polymer to the negatively charged gold nanoparticle surfaces through electrostatic interactions. Using of chitosan serves dual purpose of providing sufficient steric hindrance ensuring stability of the gold nanoparticles and also to functionalize the nanoparticles for use as sensors of heavy metals [26]. It is noteworthy a general feature of all three systems studied: the onset of nanoparticle agglomeration starts at the percolation concentration producing a decrease on the effective surface area. In the case of the heavy metal sensor, at higher gold concentrations clusters start to appear which further decrease the surface area of nanoparticles with a subsequent sensitivity decrease to Cu^{2+} ions.

A third example is application of chitosan-clay nanocomposites for anion detection [30-32]. In this case, chitosan chains are absorbed on the silicate surface of clay with a mono or bilayer configuration as a function of chitosan concentration in the clay suspension. When chitosan is in excess and in acidic aqueous media, the protonated amino groups of a second chitosan layer that do not interact with the clay layer remain available as anion-exchange sites such that the nanocomposite become a suitable system for the detection of anions. Previous potentiometric measurements used graphite-CS-clay mixtures as the working electrode with chitosan-clay ratios of 0.25:1, 0.5:1, 1:1, and 2:1 [30]. It was concluded that the sensor with 5:1 chitosan-clay nanocomposite could be used as anionic exchanger; however, it is still unknown if this concentration ratio is optimal for anion detection.

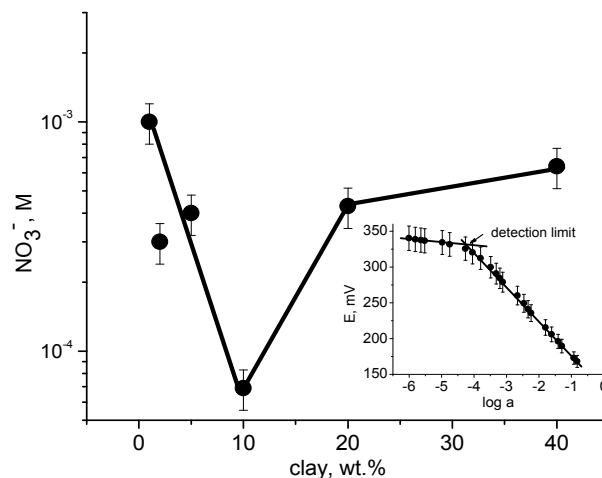


Fig. 7. Detection limits dependence of CS-bentonite film electrode toward nitrate ions as a function of membrane clay concentration. Insert shows potentiometric response to nitrate ions of electrode with a 10 wt % bentonite film. a is ion activity calculated according to ref. [29].

In this work homemade solid contact electrodes based upon graphite-epoxy with the CS-bentonite nanocomposite films have been developed as a function of bentonite wt %. Potentiometric measurements toward anions were performed with the aid of a pH-meter by using an Ag/AgCl reference electrode. The electrode potential was measured over a wide concentration range of nitrate ions from $9.9 \times$

10^{-7} M to 4.7×10^{-1} M [32]. The detection limited of electrodes was taken at the point of intersection of the two asymptotic behaviors of the calibration curve, as recommended by IUPAC (see insert on Fig. 7) [28]. Fig. 7 shows dependence of detection limit of electrode on the concentration of bentonite in films. As one can see the best detection limit has been obtained at 10 wt % of the bentonite in films, which is close to the percolation threshold (8 ± 2.5 wt %). At the percolation concentration a physical path between conductivity bentonite inclusions is formed through in which the current can flow; note that at higher clay concentration agglomeration takes place as resolved by SEM measurements. These effects promote: 1) a decrease in clay intercalation and absorption chitosan chains in the interlayer space of bentonite by ion-exchange mechanism and 2) a decrease in membrane sensitivity.

Conclusion

In this work we have developed three nanocomposites of chitosan-Ag, chitosan-Au and chitosan-clay based upon the rationale of percolation phenomena. Based upon conductivity analyses, our method allows proper comparison of different chitosan-based nanocomposites even when different preparation methods are used. With the aid of EDS analysis nanocomposite properties can be studied as a function of wt % of NPs instead of volume fraction. For first time we show that in chitosan-based nanocomposites there is a strong correlation between percolation threshold and NPs size. This observation suggests that the method of preparation and the chemical nature of NPs are not relevant as long as the proposed correlation is observed.

Impedance spectroscopy analysis helps the detection of percolation threshold values of chitosan-based nanocomposites; this percolation threshold represents a critical concentration in which a physical conductive path between NPs inclusions forms allowing the flow of current. Above the percolation concentration, NPs agglomeration takes place such that the effective surface area of the nanocomposite diminishes thus producing performance breakdown. This assertion has been confirmed by measurements of antibacterial properties of CS-AgNPs composites, sensitivity of CS-AuNPs composites for Cu^{+2} detection and sensitivity of CS-clay nanocomposite membranes for NO_3^- detection. For all these applications the best functional nanocomposite properties have been observed at NPs concentration in the vicinity of the percolation threshold. The obtained relationship between electrical, structure and concentration of nanoparticles may prove useful in the design and optimization of polymer-based nanocomposites for different applications.

Acknowledgements

This work was partially supported by CONACYT of Mexico. The authors are grateful to J.A. Muñoz-Salas for technical assistance in the impedance measurements.

Author contributions

Performed the experiments on CS- bentonite: MOM; Performed the experiments on CS- AgNPs: SKK; Performed the experiments on CS- AuNPs: EVA; Data analysis and impedance measurements: EP; Wrote the paper: EP, GLB. Authors have no competing financial interests.

Reference

- I. Jeon, Y.; Baek, J. B.; *Materials*. **2010**, *3*, 3654.
DOI: [10.3390/ma3063654](https://doi.org/10.3390/ma3063654)
- Cury Camargo, P. H.; Satyanarayana, K. G.; Wypych, F.; *Mat. Res.*, **2009**, *12*, 1.
DOI: [10.1590/S1516-14392009000100002.S1516-14392009000100002](https://doi.org/10.1590/S1516-14392009000100002.S1516-14392009000100002)
- Efros, A. L.; Shklovskii, B. I.; *Phys. Status Solidi B*, **1976**, *76*, 475.
DOI: [10.1002/pssb.2220760205](https://doi.org/10.1002/pssb.2220760205)
- Kirkpatrick, S.; *Rev Mod. Phys.*, 1973, **45**, 574.
DOI: [10.1103/RevModPhys.45.574](https://doi.org/10.1103/RevModPhys.45.574)
- Heilmann, A.; *Polymer films with embedded metal nanoparticles*; Springer: Germany, **2003**.
DOI: [10.1007/978-3-662-05233-4](https://doi.org/10.1007/978-3-662-05233-4)
- Vargas-Bernal, R.; Herrera-Pérez, G.; Calixto-Olalde, M. E.; Tecpoyotl-Torres, M.; *J. Elect& Comp Eng.*, **2013**, ID 179538.
DOI: [10.1155/2013/179538](https://doi.org/10.1155/2013/179538)
- Nan, C. W.; Shen, Y.; Ma, J.; *Annu. Rev. Mater. Res.*, **2010**, *40*, 131.
DOI: [10.1146/annurev-matsci-070909-104529](https://doi.org/10.1146/annurev-matsci-070909-104529)
- Logakis, E.; Pandis, C.; Peoglos, V.; Pissis, P.; Pionteck, J.; Pötschke, P.; Mičušík, M.; Omastová, M.; *Polymer.*, **2009**, *50*, 5103.
DOI: [10.1016/j.polymer.2009.08.038](https://doi.org/10.1016/j.polymer.2009.08.038)
- Angelov, V.; Velichkova, H.; Ivanov, E.; Kotsikova, R.; Delville, M.H.; Cangiotti, M.; Fattori, A.; *Langmuir*, **2014**, *30*, 13411.
DOI: [10.1021/la503361k](https://doi.org/10.1021/la503361k)
- Jin, Y.; Gerhardt, R. A.; *ACS Appl. Mat.& Interfaces.*, **2014**, *6*, 22264.
DOI: [10.1021/am5061239](https://doi.org/10.1021/am5061239)
- Zarate-Triviño, D. G.; Prokhorov, E.; Luna-Bárceñas, G.; et al.; *Mat. Chem. & Phys.*, **2015**, *155*, 252.
DOI: [10.1016/j.matchemphys.2015.02.041](https://doi.org/10.1016/j.matchemphys.2015.02.041)
- Xue, Q.; *Europ. Polymer J.*, **2004**, *40*, 323.
DOI: [10.1016/j.eurpolymj.2003.10.011](https://doi.org/10.1016/j.eurpolymj.2003.10.011)
- Cai, W. Z.; Tu, S. T.; Gong, J. M.; *J. Composite Mat.*, **2006**, *40*, 2131.
DOI: [10.1177/0021998306062312](https://doi.org/10.1177/0021998306062312)
- Mourya, V.K.; Inamdara, N. N.; Tiwari, A.; *Adv. Mat. Lett.*, **2010**, *1*, 11.
DOI: [10.5185/amlett.2010.3108](https://doi.org/10.5185/amlett.2010.3108)
- Honarkar, H.; Barikani, M.; *Monatsh Chem.*, **2009**, *140*, 1403.
DOI: [10.1007/s00706-009-0197-4](https://doi.org/10.1007/s00706-009-0197-4)
- Prokhorov, E.; Kumar-Krishnan, S.; Luna-Bárceñas, G.; Vazquez Lepe, M.; González Campos, B.; *Current Nanoscience*, **2015**, *11*, 166.
DOI: [10.2174/1573413710666141013223549](https://doi.org/10.2174/1573413710666141013223549)
- González-Campos, J. B.; Prokhorov, E.; Luna-Bárceñas, G.; Sanchez, I.C.; Lara-Romero, J.; Mendoza-Duarte, M. E.; *J. Polym Sci: Part B.*, **2010**, *48*, 739.
DOI: [10.1002/polb.21941](https://doi.org/10.1002/polb.21941)
- Huang, X.; Jiang, P.; Xie, L.; *Appl. Phys. Lett.*, **2009**, *95*, 242901.
DOI: [10.1063/1.3273368](https://doi.org/10.1063/1.3273368)
- Bakeeva, I.V.; Kolesnikova, Y.A.; Kataeva, N.A.; Zaustinskaya, K.S.; Gubin, S.P.; Zubov, V.P.; *Russ. Chem. Bull.*, **2008**, *57*, 337.
DOI: [10.6666/08/5702-0337](https://doi.org/10.6666/08/5702-0337)
- Bouvier, A.; Feller, J.F.; Castro, M.; Grohens, Y.; Rinaudo, M.; *Sensors and Actuators B*, **2009**, *138*, 138.
DOI: [10.1016/j.snb.2009.02.022](https://doi.org/10.1016/j.snb.2009.02.022)
- Zarate-Triviño, D.G.; Valenzuela Acosta, E.M.; Prokhorov, E.; Luna-Bárceñas, G.; Rodríguez Padilla, C.; Franco Molina, M. A.; *Nano Material, Appl & Prop*, **2013**, *2*, 04NABM01-1.
DOI: [doaj.org/toc/2306-580X/2](https://doi.org/10.1002/2306-580X/2)
- Potara, M.; Jakab, E.; Damert, A.; Popescu, O.; Canpean, V.; Astilean, S.; *Nanotechnology*, **2011**, *22*, 135101.
DOI: [10.1088/0957-4484/22/13/135101](https://doi.org/10.1088/0957-4484/22/13/135101)
- Kumar-Krishnan, S.; Prokhorov, E.; Hernández-Iturriaga, M.; Mota-Morales, J. D.; Vázquez Lepe, M.; Kovalenko, Y.; Sanchez, I.C.; Luna-Bárceñas, G.; *Europ. Polym. J.*, **2015**, *67*, 242.
DOI: [10.1016/j.eurpolymj.2015.03.066](https://doi.org/10.1016/j.eurpolymj.2015.03.066)
- Jiang, X.C.; Chen, W.M.; Chen, C.Y.; Xiong S.X.; Yu, A.B.; *Nanoscale. Res. Lett.*, **2011**, *6*, 32.
DOI: [10.1007/s11671-010-9780-1](https://doi.org/10.1007/s11671-010-9780-1)
- Sugunan, A.; Thanachayanont, C.; Dutta, J.; Hilborn, J.G.; *Sci&Techn Adv. Mat.*, **2005**, *6*, 335.

- DOI: [10.1016/j.stam.2005.03.007](https://doi.org/10.1016/j.stam.2005.03.007)
26. Praig, V.G.; Mellwee, H.; Schauer, C.L.; Boukherroub, R.; Szunerits, S.; *J. Nanosci. Nanotechnol.*, **2009**, 9, 350.
DOI: [10.1166/jnn.2009.J064](https://doi.org/10.1166/jnn.2009.J064)
27. Mathew, M.; Sureshkumar, S.; Sandhyarani, N.; *Colloids&Surf. B: Biointerfaces.*, **2012**, 93, 143.
DOI: [10.1016/j.colsurfb.2011.12.028](https://doi.org/10.1016/j.colsurfb.2011.12.028)
28. Umezawa, Y.; Umezawa, K.; Tohda, K.; Amemiya, S.; *Pure Appl. Chem.*, **2000**, 72, 1851.
DOI: [10.1351/pac200072101851](https://doi.org/10.1351/pac200072101851)
29. Meier, P. C.; *Anal. Chim. Acta.*, **1982**, 136, 363.
DOI: [10.1016/S0003-2670\(01\)95397-8](https://doi.org/10.1016/S0003-2670(01)95397-8)
30. Darder, M.; Colilla, M.; Ruiz-Hitzky, E.; *Chem. Mater.*, **2003**, 15, 3774.
DOI: [10.1021/cm0343047](https://doi.org/10.1021/cm0343047)
31. Darder, M.; Colilla, M.; Ruiz-Hitzky, E.; *Appl. Clay Sci.*, **2005**, 28, 199.
DOI: [10.1016/j.clay.2004.02.009](https://doi.org/10.1016/j.clay.2004.02.009)
32. Oviedo Mendoza, M.; Arias de Fuentes, O.; Prokhorov, E.; Luna Barcenas, G.; Padilla Ortega, E.; *Adv. Mat. Sci.& Eng.*, **2015**, 215, 710425.
DOI: [10.1155/2015/710425](https://doi.org/10.1155/2015/710425)

Advanced Materials Letters

Copyright © 2016 VBRI Press AB, Sweden
www.vbripress.com/ami

A Monthly Journal

Publish your article in this journal

Advanced Materials Letters is an official international journal of International Association of Advanced Materials (IAAM, www.iaamonline.org) published monthly by VBRI Press AB from Sweden. The journal is intended to provide high-quality peer-review articles in the fascinating field of materials science and technology particularly in the area of structure, synthesis and processing, characterisation, advanced-state properties and applications of materials. All published articles are indexed in various databases and are available download for free. The manuscript management system is completely electronic and has fast and fair peer-review process. The journal includes review article, research article, notes, letter to editor and short communications.



VBRI Press
a rapid publication platform